Journal of The Electrochemical Society, **158** (3) P37-P40 (2011)
0013-4651/2011/158(3)/P37/4/$28.00 © The Electrochemical Society

Effect of Crystallinity on the Optical Reflectance of Cylindrical Colloidal Crystals

Chun-Han Lai,[a] Yu-Lin Yang,[b] Li-Yin Chen,[a] Yi-Jui Huang,[a] Jing-Yu Chen,[a] Pu-Wei Wu,[a,*,z] Yu-Ting Cheng,[b] and Yang-Tung Huang[b]

[a]Department of Materials Science and Engineering, and [b]Department of Electronics Engineering, National Chiao Tung University, Hsin-chu 300, Taiwan

We fabricate cylindrical colloidal crystals (CCCs) via electrophoretic depositions of polystyrene microspheres on a carbon fiber in a concentric arrangement. Images from optical and scanning electron microscope indicate that the CCCs of 460 nm microspheres reveal a semicrystalline structure in close-packed lattice, while the CCCs of 660 exhibit an amorphous arrangement. In optical reflectance spectra, both CCCs demonstrate a dispersive photonic bandgap as compared to that from planar counterparts. The curved contour for the CCCs renders incident light interacting with reflecting planes at slightly different angles, leading to a notable reduction in the reflectance intensity and minor relocation of photonic bandgap contingent on their crystallinity.
 [DOI: 10.1149/1.3536511]

Manuscript submitted September 23, 2010; revised manuscript received November 4, 2010. Published January 20, 2011.

Photonic crystals are three-dimensional periodic arrays of dielectric materials that exhibit a photonic bandgap in which certain frequencies of electromagnetic waves are forbidden to propagate.[1,2] This unique character can be applied for many devices in optical and optoelectronic applications such as wave guides, solar cells, LED, etc.[3-5] The concept of photonic crystals was first proposed in 1987 by Yablonovitch[6] and John[7] independently for inhibiting spontaneous emission and localization of photons. It was later understood that the photonic crystals could also be employed to direct light flow by creating two-dimensional and three-dimensional defects within.[8] To date, considerable efforts have been devoted to design and construct photonic crystals in various structures using metals, polymers, and dielectrics with the objective to achieve a complete photonic bandgap in the optical regime.[9-13]

Conventional fabrication methods for the photonic crystals entail schemes of microfabrication (top-down) and self-assembly of colloidal microspheres (bottom-up).[14,15] The microfabrication approach involves standard semiconductor processing protocols that allow the construction of photonic crystals on Si platforms with a desirable periodicity and superb crystallinity. In contrast, the self-assembly route adopts a wet chemical technique where colloidal microspheres are assembled in a close-packed structure via sedimentation, solvent evaporation, or electrophoresis.[16-21] However, the photonic crystals from both the fabrication methods are often prepared in planar forms with well-defined periodic constituents that reveal a photonic bandgap with narrow bandwidth. Previously, Lin et al.[22,23] demonstrated the fabrication of the photonic crystals in a cylindrical configuration by infiltrating microspheres in a tubular vessel forming close-packed cylindrical colloidal crystals (CCCs) within. Results from optical measurements for those CCCs indicated that the photonic bandgap is determined by the ordered colloidal layers on their surface, similar to that of planar colloidal crystals.

Recently, we adopted a combination of electrophoresis and electrodeposition to fabricate CCCs and their inverse opals in a relatively short process time.[24] Using a carbon fiber (CF) as the substrate, we assembled polystyrene (PS) microspheres concentrically outward to form the CCCs with various diameters. By selecting proper microsphere size (460 and 660 nm), we were able to obtain the CCCs in both semicrystalline and amorphous states. In this work, we conduct reflectance measurements on both the CCCs to investigate the structural effect on the resulting optical characteristics. For comparison purpose, we also construct planar colloidal crystals using identical microspheres to obtain their respective reflectance spectra.

* Electrochemical Society Active Member.
z E-mail: ppwu@mail.nctu.edu.tw

Experimental

To construct the CCCs, a CF (TORAYCA-T300) with 7 μm diameter and 2.5 cm length was employed as the substrate. PS microspheres of 460 and 660 nm diameter were first suspended in ethanol followed by electrophoretic assembly on the CF in a concentric arrangement. The duration for the electrophoresis was adjusted to obtain CCCs with different diameters. Subsequently, the samples were carefully removed from the suspension and dried at 25°C. To explore their internal structure, the CCCs underwent a potentiostatic electroplating to deposit Ni within the interstitial voids among the PS microspheres. Afterward, the PS microspheres were dissolved in an ethylene acetate solution to obtain Ni inverse opals. Detailed information on the synthesis of PS microspheres, experimental setup for the CCCs and their inverse opals, as well as relevant processing parameters can be found elsewhere.[24]

Optical pictures for the CCCs were taken by a microscope (Olympus CX41). Cross-sectional images for the Ni inverse opals were obtained using a scanning electron microscope (SEM, JEOL-LSM-6700F). The photonic bandgap for the CCCs at various diameters was determined from reflectance spectra for wavelengths between 1 and 1.8 μm using a Fourier transform infrared (FTIR) spectrometer (Hyperion 2000, Bruker). The samples were fixated on a glass substrate, which was inactive in the near infrared region, and the area under FTIR beam size was adjusted to cover the entire CCCs. For comparison purpose, we also prepared planar colloidal crystals by electrophoresis of PS microspheres on a tin-doped indium oxide coated glass and recorded their reflectance characteristics. Similar preparation steps for the planar colloidal crystals using SiO_2 microspheres have been reported earlier.[25] The reflectance measurement setups for both planar and cylindrical samples are presented in Fig. 1.

Results and Discussion

Figure 2 demonstrates the optical pictures of CCCs assembled with PS microspheres of 460 and 660 nm after electrophoresis of 10 min. Their diameter was 304.6 and 230.1 μm, which corresponded to the colloidal layers of 373 and 195, respectively. These values were obtained by the following equation. In a planar colloidal crystal with multiple colloidal layers

$$N = \frac{(T - r)}{r} \times \frac{3}{2\sqrt{6}} + 1 \qquad [1]$$

where N is the number of layers, T is the thickness for the colloidal crystal, and r is the radius of PS microspheres. In our samples, because the diameter for the cylindrical colloidal crystal is much larger than the radius of PS microspheres, the colloidal layers are considered parallel to each other so that the equation above can be applied. A shown in Fig. 2, both samples exhibited a considerable

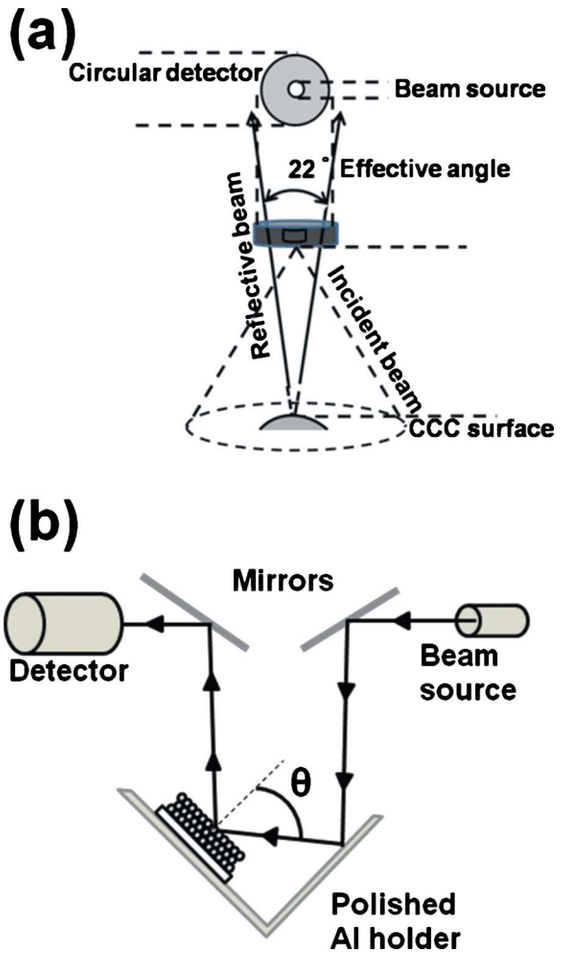

Figure 1. (Color online) Measurement setups for reflectance spectra of (a) CCCs and (b) planar colloidal crystals (the θ is the angle between the incident beam and normal to the (111) plane of the colloidal crystals).

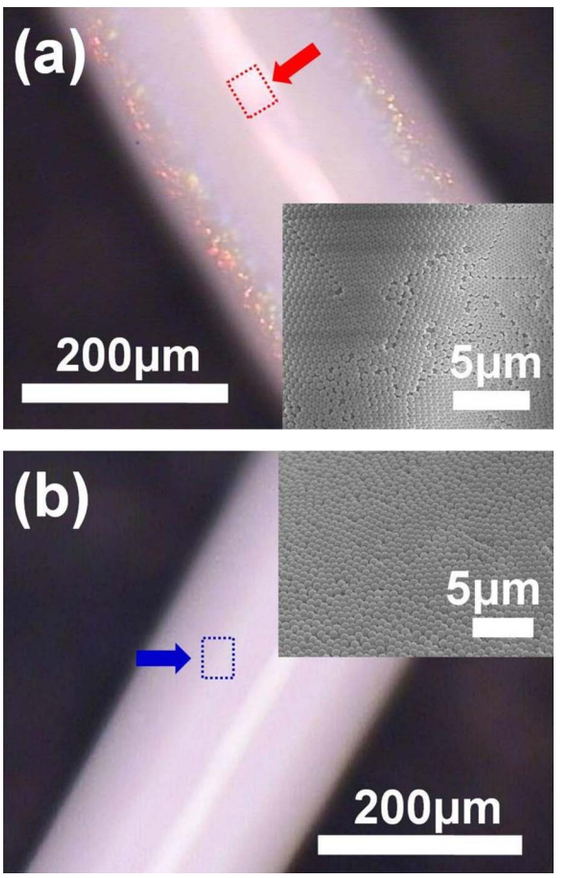

Figure 2. (Color online) Optical pictures for the CCCs of (a) 460 and (b) 660 nm PS microspheres after electrophoretic depositions of 10 min. Shown in the insets are their respective SEM images taken from the area identified in the optical pictures.

uniformity for the entire length. Insets in Fig. 2 are their SEM images for the area identified on the optical pictures. From the SEM images, the CCCs of 460 nm microspheres revealed a semicrystalline structure in close-packed face-centered cubic (fcc) lattice (111) with scattered vacancies and grain boundaries. The inability to form a nicely arranged close-packed lattice is not unexpected because the CF itself was not entirely smooth on the surface, and the packing of colloids was affected greatly by the substrate condition. Nevertheless, the crystallinity for the CCCs of 460 nm was significantly better than that of 660 nm CCCs that displayed an amorphous arrangement. In colloidal assembly, we rationalized that smaller microspheres were able to pack better than larger ones on a curved surface, so, the CCCs of 460 nm exhibited a semicrystalline configuration instead of amorphous structure. This improved crystallinity that can also be inferred from the formation of iridescent fringes on the CCCs of 460 nm, as shown in Fig. 2a. A similar phenomenon was observed by Rastogi et al.[26] in their study of spherical colloidal crystals, and they attributed those fringes to the light diffraction from the ordered domains of microspheres. In the central area, the incoming light was directly reflected; hence, this behavior was analogous to the reflectance from a planar colloidal crystal. In contrast, in the edge, the curved surface rendered a minute variation in the incident angle, leading to a scattered reflected light. As a result, we observed a darker area on the perimeter.

It is recognized that the structural arrangements in the radial direction for the CCCs could be confirmed via the observation of their inverse opals after removing the PS template. To achieve this objective, we chose the Ni to fabricate the inverse structure. In our observations, the electrodeposited Ni revealed impressive chemical stability and mechanical integrity so that the sample was expected to experience a negligible damage in the fabrication of inverse structure. Figure 3 presents the cross-sectional SEM images for the inverse opals from the CCCs of 460 and 660 nm microspheres. The inset in Fig. 3a provides an illustration on the location where these SEM images were taken. Consistent with what we observed in Fig. 2, the inverse opals of 460 nm microspheres demonstrated a hexagonal structure while the inverse opals of 660 nm microspheres, shown in Fig. 3b, revealed a random pattern. As a result, we expected to obtain minor differences in both photonic bandgap and bandwidth between these two samples.

Figure 4 exhibits the reflectance spectra of CCCs obtained at various electrophoretic deposition times. Because the deposition rate for the 460 nm microspheres was higher than that of the 660 nm ones, the diameter for the CCCs of the 460 nm microspheres was larger than the 660 nm ones for a given deposition time. The spectra from planar colloidal crystals were also included in the insets for comparison. The peak positions for the planar colloidal crystals of the 460 and 660 nm microspheres were 1089 and 1627 nm, respectively. In addition, their reflectance intensities were relatively strong. These results substantiate that the electrophoresis process is able to produce colloidal crystals with photonic bandgap that is well-defined and consistent with estimation from Bragg's diffraction law.

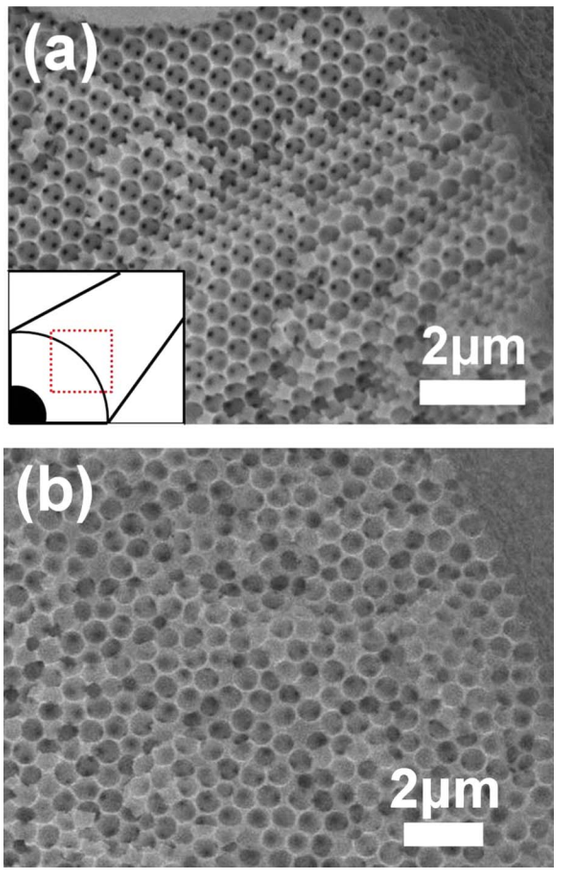

Figure 3. (Color online) SEM images of the Ni skeleton for the CCCs of (a) 460 and (b) 660 nm PS microspheres. Shown in the inset of (a) is the illustration for the SEM image.

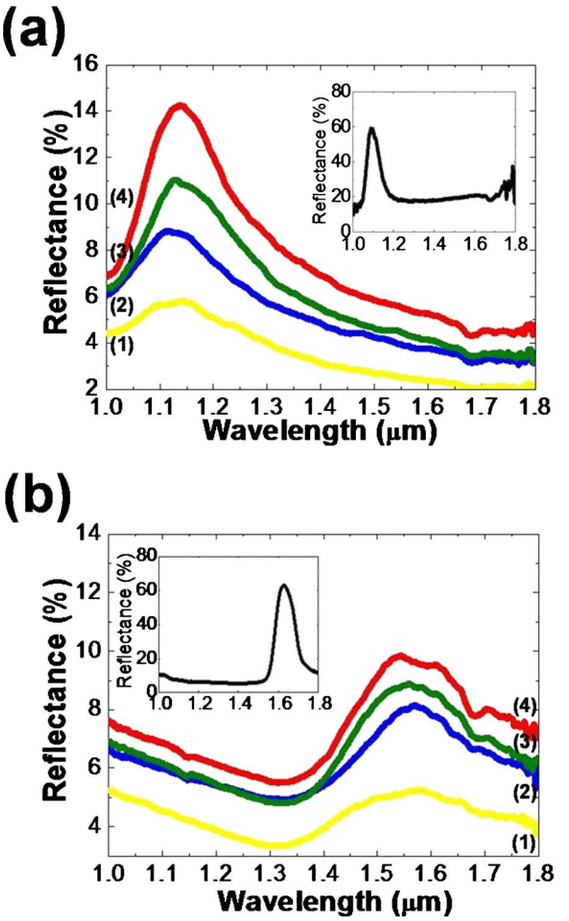

Figure 4. (Color online) Reflectance spectra recorded from the CCCs of (a) 460 and (b) 660 nm PS microspheres obtained after electrophoretic deposition time of (1) 2, (2) 6, (3) 8, and (4) 10 min, respectively. Their resulting CCCs diameters were between 84 and 373 μm. Shown in the insets are the reflectance spectra of planar colloidal crystals for comparison purpose. The thickness for planar colloidal crystal was 94 (460 nm microspheres) and 58 μm (660 nm microspheres), respectively.

From literature, the peak position for the photonic bandgap (the wavelength with the highest reflectance) from a planar colloidal crystal can be estimated by following equations[27]

$$\lambda_c = 2 \times n_{eff} \times d \quad [2]$$

$$n_{eff}^2 = n_s^2 \times f + n_{air}^2 \times (1 - f) \quad [3]$$

where λ_c is the wavelength for the peak position, n_{eff} is the effective refractive index of the colloidal crystal, d is the lattice spacing for the (111) plane, f is the filling factor for a close-packed lattice, which is 0.74, n_s is the refractive index of PS, and n_{air} is the refractive index of air. Therefore, the position of the photonic bandgap for the 460 and 660 nm microspheres were expected to occur at 1104 and 1573 nm, respectively. These values were reasonably close to what we measured at 1089 and 1627 nm in the reflectance spectra.

To estimate the photonic bandgap for CCCs using Eq. 2 and 3, minor adjustments of f and d are necessary. On a curved substrate, the value of f is expected to become smaller than 0.74 because the circumference changes with radial distance and, in each concentric layer, extra space is required to accommodate colloid packing on a curved contour. As a result, from Eq. 3, one would expect the CCCs to reveal a lower n_{eff}, which leads to a shorter wavelength for the photonic bandgap. On the other hand, the value of d for the CCCs is likely to be stretched moderately for the same reason as opposed to that in a close-packed planar counterpart. Hence, from Eq. 2, one would expect to observe a redshift of photonic bandgap accordingly. Apparently, these two trends counteract each other, rendering the photonic bandgap rather sensitive in overall crystallinity and presence of defects.

For the CCCs of the 460 nm microspheres, as shown in Fig. 4a, the peak positions were located at 1114–1136 nm with a slight variation with the increasing thickness. Relative to that of planar colloidal crystals (1104 nm), these peak positions were notably redshifted. Therefore, we rationalized that the increase of d predominated over the slight reduction in f, resulting in a photonic bandgap of longer wavelengths. This was likely because the CCCs of 460 nm were confirmed by the SEM image in Fig. 2a to exhibit a semicrystalline structure. However, for the CCCs of 660 nm microspheres, their photonic bandgap were blueshifted (1544–1575 nm) relative to that of planar colloidal crystals (1627 nm). Because the CCCs of 660 nm were established to reveal an amorphous nature, the actual filling factor was considerably lower than 0.74 while the value of d was likely to remain relatively unchanged. This led to a photonic bandgap with a shorter wavelength. For both CCCs, we did not obtain the reflectance spectra from different incident angles because the CCCs were axisymmetric and earlier work by Míguez et al.[27] had confirmed the angular invariance of the photonic bandgap.

From Fig. 4, it can be seen that the strength of photonic bandgap for both CCCs was also affected by the number of colloidal layers. In both samples, their reflectance intensities were proportional to the CCC thickness, which were reasonably expected because not only the number of reflecting planes but also the area contributing to the

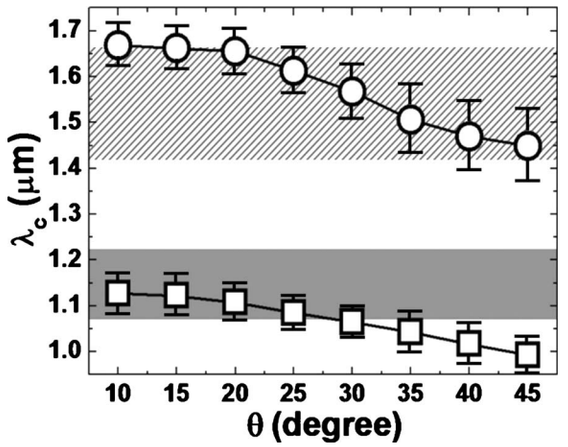

Figure 5. Angular dependence of photonic bandgap (λ_c) from planar colloidal crystals of 460 (□) and 660 nm (○) PS microspheres, respectively. The error bar associated with each data is its respective fwhm. The shaded area is the fwhm of photonic bandgap from the corresponding CCCs.

reflection intensity increased with the increasing thickness. However, the intensities for the reflection signals were considerably lower as opposed to those from planar colloidal crystals. We realized that due to the curved surface on the CCCs, the reflected light was likely to be dispersive in space, reducing the amount arriving at the detector.

Another notable feature from the CCCs was that the full width at half-maximum (fwhm: $\Delta\lambda$) for the reflection signals was considerably broader than those recorded from the planar colloidal crystals. In a model provided by Tarhan and Watson,[28] the value of $\Delta\lambda/\lambda_c$ for an fcc photonic crystal from the (111) planes is 0.054. In our CCCs, we obtained $\Delta\lambda/\lambda_c$ values in the range of 0.139–0.152. We surmised that this dispersive nature was possibly caused by the local variation in the incident angle with respect to the reflecting planes. To substantiate our assumption, we measured the reflectance spectra of planar colloidal crystals at different incident angles (θ) and recorded the resulting λ_c value. Figure 5 demonstrates the variation of λ_c as a function of θ. Also provided are the fwhm for each data point labeled as error bar. The shaded areas in Fig. 5 exhibit the fwhm of CCCs from Fig. 4a-(4) to Fig. 4b-(4), respectively. As shown in Fig. 5, when the incident angle was increased, the λ_c became blueshifted correspondingly. This behavior agreed well with earlier work by Míguez et al.[27] on the angular dependence of λ_c. For the 460 nm sample, the variation of λ_c coincided with the shaded area of 460 nm. Therefore, we realized that the broad fwhm from the CCCs of 460 nm was attributed to mixtures of Bragg signals from different incident angles. In addition, because the incident beam was normal to the CCCs surface, the majority of signals were received from the area within a finite incident angle. This effect became more pronounced for the CCCs of 660 nm because their amorphous structure compromised the effect of incident angle. As a result, the contribution of fwhm for the CCCs of 660 nm was primarily from the lattice spacing with incident angles less than 30°.

Conclusions

We fabricated the CCCs via electrophoretic depositions of PS microspheres on a CF in a concentric arrangement. The CCCs of 460 nm microspheres revealed a semicrystalline structure while the CCCs of 660 exhibited an amorphous nature. It is because the PS microspheres with a smaller size allow them to pack in an ordered arrangement over a curved substrate. In reflectance spectra, both CCCs demonstrated a dispersive photonic bandgap with a fwhm of 200–400 nm in conjunction with a reduced reflectance as compared to those of planar colloidal crystals. In addition, relocation of photonic bandgap was observed. The photonic bandgap was found to redshift for the CCCs of 460 nm and blueshift for the CCCs of 660 nm resulting from combined effects of lattice spacing and packing defects.

Acknowledgment

Financial support from the National Science Council of Taiwan (98-2221-E-009-040-MY2) is acknowledged. Equipment loan from Professor George Tu and Professor Pang Lin are greatly appreciated.

National Chiao Tung University assisted in meeting the publication costs of this article.

References

1. E. Yablonovitch, *J. Mod. Phys.*, **41**, 173 (1994).
2. A. Moroz and C. Sommers, *J. Phys.: Condens. Matter*, **11**, 997 (1999).
3. D. M. Beggs, L. O'Faolain and T. F. Krauss, *Photonics Nanostruct. Fundam. Appl.*, **6**, 213 (2008).
4. S. Guldin, S. Huttner, M. Kolle, M. E. Welland, P. Muller-Buschbaum, R. H. Friend, U. Steiner, and N. Tetreault, *Nano Lett.*, **10**, 2303 (2010).
5. D. H. Long, I. K. Hwang and S. W. Ryu, *IEEE J. Sel. Top. Quantum Electron.*, **15**, 1257 (2009).
6. E. Yablonovitch, *Phys. Rev. Lett.*, **58**, 2059 (1987).
7. S. John, *Phys. Rev. Lett.*, **58**, 2486 (1987).
8. J. D. Joannopoulos, R. D. Meade, and J. N. Winn, *Photonic Crystals*, Princeton University, Princeton, NJ (1995).
9. Y. W. Hao, F. Q. Zhu, C. L. Chien, and P. C. Searson, *J. Electrochem. Soc.*, **154**, D65 (2007).
10. Y. L. Yang, F. J. Hou, S. C. Wu, W. H. Huang, M. C. Lai, and Y. T. Huang, *Appl. Phys. Lett.*, **94**, 041122 (2009).
11. Y. W. Chung, I. C. Leu, J. H. Lee, and M. H. Hon, *J. Electrochem. Soc.*, **156**, E91 (2009).
12. Z. Wang, M. A. Fierke, and A. Stein, *J. Electrochem. Soc.*, **155**, A658 (2008).
13. S. Y. Lin, J. G. Fleming, D. L. Hetherington, B. K. Smith, R. Biswas, K. M. Ho, M. M. Sigalas, W. Zubrzycki, S. R. Kurtz, and J. Bur, *Nature (London)*, **394**, 251 (1998).
14. J. H. Lee, Y. S. Kim, K. Constant, and K. M. Ho, *Adv. Mater. (Weinheim, Ger.)*, **19**, 791 (2007).
15. Á. Blanco and C. López, *J. Mater. Chem.*, **16**, 2969 (2006).
16. L. C. K. Liau and Y. K. Huang, *Expert Sys. Applic.*, **35**, 887 (2008).
17. J. Xu, J. F. Xia, S. W. Hong, Z. Q. Lin, F. Qiu, and Y. L. Yang, *Phys. Rev. Lett.*, **96**, 066104 (2006).
18. P. Granitzer, K. Rumpf, M. Venkatesan, A. G. Roca, L. Cabrera, M. P. Morales, P. Poelt, and M. Albu, *J. Electrochem. Soc.*, **157**, K145 (2010).
19. M. A. Ray, H. Kim, and L. Jia, *Langmuir*, **21**, 4786 (2005).
20. J. Xu, J. Xia, and Z. Lin, *Angew. Chem., Int. Ed.*, **46**, 1860 (2007).
21. M. Byun, J. Wang, and Z. Lin, *J. Phys.: Condens. Matter*, **21**, 264014 (2009).
22. Y. Lin, P. R. Herman, C. E. Valdivia, J. Li, V. Kitaev, and G. A. Ozin, *Appl. Phys. Lett.*, **86**, 121106 (2005).
23. Y. K. Lin, P. R. Herman, and W. Xu, *J. Appl. Phys.*, **102**, 073106 (2007).
24. C. H. Lai, Y. J. Huang, P. W. Wu, and L. Y. Chen, *J. Electrochem. Soc.*, **157**, P23 (2010).
25. Y. J. Huang, C. H. Lai, and P. W. Wu, *Electrochem. Solid-State Lett.*, **11**, P20 (2008).
26. V. Rastogi, S. Melle, O. G. Calderón, A. A. Garciá, M. Marquez, and O. D. Velev, *Adv. Mater. (Weinheim, Ger.)*, **20**, 4263 (2008).
27. H. Míguez, C. López, F. Meseguer, A. Blanco, L. Vázquez, R. Mayoral, M. Ocaña, V. Fornés, and A. Mifsud, *Appl. Phys. Lett.*, **71**, 1148 (1997).
28. I. I. Tarhan and G. H. Watson, *Phys. Rev. B*, **54**, 7593 (1996).